Accepted Manuscript

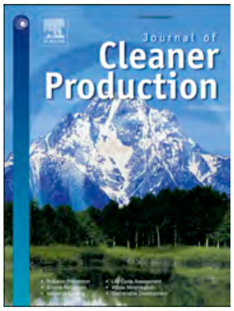

Analysis of a domestic trigeneration scheme with hybrid renewable energy sources and desalting techniques

Javier Uche, Luis Acevedo, Fernando Círez, Sergio Usón, Amaya Martínez-Gracia, Ángel Antonio Bayod-Rújula

PII: S0959-6526(18)33708-9

DOI: https://doi.org/10.1016/j.jclepro.2018.12.006

Reference: JCLP 15064

To appear in: *Journal of Cleaner Production*

Received Date: 7 June 2018

Revised Date: 19 November 2018

Accepted Date: 1 December 2018

Please cite this article as: Uche J, Acevedo L, Círez F, Usón S, Martínez-Gracia A, Bayod-Rújula ÁAntonio, Analysis of a domestic trigeneration scheme with hybrid renewable energy sources and desalting techniques, *Journal of Cleaner Production* (2019), doi: https://doi.org/10.1016/j.jclepro.2018.12.006.

Amount of words: 9937

Analysis of a domestic trigeneration scheme with hybrid renewable energy sources and desalting techniques

Javier Uche*[1], Luis Acevedo[2], Fernando Círez[3], Sergio Usón[4], Amaya Martínez-Gracia[5], Ángel Antonio Bayod-Rújula[6]

[1] Department of Mechanical Engineering, University of Zaragoza, Spain. javiuche@unizar.es

[2] Process Integration Group, CIRCE Foundation, Zaragoza (Spain). lacevedo@fcirce.es

[3] Process Integration Group, CIRCE Foundation, Zaragoza (Spain). fcirez@fcirce.es

[4] Department of Mechanical Engineering, University of Zaragoza, Spain. suson@unizar.es

[5] Department of Mechanical Engineering, University of Zaragoza, Spain. amayamg@unizar.es

[6] Department of Electrical Engineering, University of Zaragoza, Spain. aabayod@unizar.es

Corresponding Author e-mail: javiuche@unizar.es

Abstract

In this paper, experimental tests of a hybrid trigeneration pilot unit based on renewable energy sources are presented and analysed. The plant provides electricity by coupling four photovoltaic/thermal collectors and a micro-wind turbine, fresh water by means of hybrid desalination (membrane distillation, and reverse osmosis), and sanitary hot water coming from the photovoltaic/thermal collectors and an evacuated tubes collector. Plant design was previously modeled to cover the power, freshwater and sanitary hot water for a typical family home (four residents) isolated from the power and water networks. The hybrid pilot unit has been tested from May 2017 to March 2018 in Zaragoza (Spain). Results from those tests show that daytime assessment of power, freshwater and sanitary hot water produced allowed a good coverage of scheduled energy and water demands. Flexible operation due to the combined production of power and heat was also observed. State of charge of the batteries and the temperature of the sanitary hot water tank are the key control variables, which allow to give priority to power, freshwater or sanitary hot water production according to the ordered demands or economic incentives. Environmental assessment of the pilot unit along its life cycle also has shown very low impacts with respect to the conventional supply of energy and water.

Nomenclature

A – Area
AC – Alternating Current / Air Cooled
ANN – Artificial Neural Network
B – Bias
C – Conductivity
Cp – Specific heat
CR – Coverage Rate
CSP – Concentrated Solar Power
CW – Cooling Water
DC – Direct Current
E – Electricity
ED – Electrodialysis
ER – Electric Resistance
ETC – Evacuated Tube Collector

F – Flow rate
FPC – Flat Plate Collector
FW – Fresh Water (by seawater desalination)
G – Irradiation
HVAC – Heating, Ventilating and Air Conditioning systems
HWT – Hot Water Tank
HX – Heat exchanger
I – Intensity
LCA – Life Cycle Analysis
LCI – Life Cycle Inventory
LCIA – Life Cycle Impact Assessment
m – Mass flow rate
MD – Membrane Distillation
MED – Multi-Effect Distillation
MPPT – Maximum Power Point Tracker
MSF – Multi Stage Flash distillation
ORC – Organic Rankine Cycle
P – Precision / Pump
PC – Personal Computer
PG – Permeate Gap (membrane distillation type)
PTC – Parabolic Through Collector
PV – Photovoltaic
PVT – Photovoltaic/Thermal collector
Q – Heat
r – Calculated value (from several measurements)
RO – Reverse Osmosis
RR – Recovery Ratio
RES – Renewable Energy Sources
SEC – Specific Energy Consumption
SHW – Sanitary Hot Water
SOC – State of Charge
SWT – Sea Water Tank
T – Temperature
TDS – Total Dissolved Solids
U – Uncertainty
v – Velocity
V – Voltage
W – Power
WHO – World Health Organization
WT – Wind Turbine
X – Experimental measurement

Subscripts
av – averaged
cn – condenser (MD)
d – distillate
e – electrical
ev – evaporator (MD)
g – global
h – home
i – inlet
o – outlet
p – permeate
RE – renewable
S – solar
sl – solar loop

t – thermal
tw – tap water
w – water
X – measured variable

1. Introduction

The search of innovative, integrated and sustainable solutions to provide secure energy and water for population is an emerging issue. In isolated areas where power and water networks induce economic and environmental extra costs, this search should be stressed. Water and energy nexus is a key challenge not only in developing countries and dry areas (Brandoni and Bosnjakovic, 2017). In this coupling, the use of renewable energy sources (RES) is one affordable option for the future of the water cycle in urban areas (Durin and Margeta, 2014) even in oil rich countries (Caldera et al., 2018) where seawater or brackish desalination is the only source that feeds the cycle.

RES are now a widely extended sustainable solution that can be easily adapted to cover specific or local demands. Many examples can be found in literature, including some reviews for solar power and heat (Modi et al., 2017) or solar desalination (Kalogirou, 2005) and wind energy for domestic purposes (Tummala and Velamati, 2016). In case of not having abundant solar irradiance, a wind-solar hybrid system is commonly utilized in isolated areas since electricity generated can greatly meet the load demands because one energy device can offset the shortfall of the other during the daytime and nighttime respectively (Bakic et al., 2012; Huang et al, 2015). Sometimes, geothermal or biomass energy substitutes the wind supply (Al-Ali and Dincer, 2015; Srinivas and Reddy, 2014). Within solar energy, both electricity and thermal energy can be obtained through the use of a photovoltaic-thermal collector (PVT) (Liang et al., 2015). This hybrid collector integrates features of single photovoltaic and solar thermal systems in one combined product (cogeneration). Due to electricity and thermal energy production of PVT, economic and space savings are twice than utilizing the single PV module (Buonomano et al., 2016). Experimental tests including previous design and further validation of diverse PVT installations can also be found in literature (Zhou et al., 2017; Del Amo et al., 2017).

On the other hand, one of the major problems found in dry and/or isolated areas is water scarcity. Desalination of seawater and brackish water is maybe the unique solution to alleviate freshwater (FW) scarcity nowadays (Gao et al., 2017). However, it is an energy intensive process, since distillation processes such as multi-stage Flash (MSF), multi-effect distillation (MED) and membrane distillation (MD) can consume about 50–70, 40–60 and 120–1700 kWh of thermal energy per cubic meter of distillate, respectively. Membrane techniques such as reverse osmosis (RO) can consume about 3 to 6 kWh of electricity per cubic meter of permeate (González et al., 2017), being electrodialysis (ED) constrained to desalt brackish waters. Distillation processes also involve some power consumption related to pumping seawater, distillate and brine flows. The use of RES in desalination has also been extensively analyzed and modeled (Koroneos et al., 2007; Gude, 2015; Al-Karaghouli and Kazmerski, 2013) for several desalination technologies, being RO the most extended technology (Rym et al., 2016; Salcedo et al., 2012) and MED the distillation alternative for big plant desalting capacities only supplied by solar energy since water scarce areas usually exhibit the highest solar energy presence (Ortega et al., 2016; Palenzuela et al., 2015; Sharan and Bandyopathyay, 2017; Sharaf et al., 2012). However, membrane distillation (MD) is appropriate for small capacities and isolated areas (Banat and Jwaied, 2008; Chang et al., 2012; Zaragoza et al., 2014). Therefore, several solar MD configurations have been analyzed and/or tested as a sustainable local solution (Shim et al., 2015; Chen et al., 2012; Elzahaby et al., 2016; Kabeel et al., 2017; Kim et al., 2013; Raluy et al., 2012). In this sense, the use of solar energy to distillate salty waters at a reduced scale can also be obtained by alternative devices like solar stills (Manokar et al., 2018) or ad-hoc designs based on evaporation/condensation (Trujillo et al., 2014), although lower performances are usually found.

Hybrid RES schemes have been usually combined in order to provide a continuous and safe supply to desalination facilities. In this sense, several techniques (RO, MED, MD) have been coupled with diverse hybrid RES schemes (solar, wind, biomass) in both theory (Cherif and Beldadj, 2011) and practice (Chafidz et al., 2016; Weiner et al., 2001). Alternatively, hybrid desalination has been also promoted in order to provide a constant supply of fresh water from fossil fuels (Mokhtari et al., 2016; Rensonnet et al., 2007), being concentrated solar power (CSP) the large-scale solar alternative to PVT that can provide heat and power to desalination systems (Iaquaniello et al., 2014).

Regarding the multi-purpose generation or polygeneration that includes desalted water among its products, several combinations based on fossil fuels have been proposed in literature (Jana et al., 2017; Maraver et al., 2012; Serra et al., 2009). The use of a unique RES has been recently introduced in the sustainable analysis of the joint production of energy (power, heat, cooling or H_2) and water (Demir and Dincer, 2017; Leiva et al., 2017; Mohan et al., 2016a; Naseri et al., 2017; Rubio et al., 2011) and was experimentally analyzed in Mohan et al. (2016b). Besides, the combined use of hybrid RES or PVTs to provide a multipurpose scheme including desalination is rather unusual and only restricted to feasibility, exergo-economic analysis and/or optimization (Ahmadi et al., 2014; Calise et al., 2014, 2015, 2016; Rahsidi and Khorsidi, 2018; Sahoo et al., 2015).

This state of the art denotes that, apart from producing RES or water with hybrid techniques separately, there are very few examples of tri-generation or poly-generation schemes involving seawater desalination and RES, and even less if the hybrid production of electricity and water can be complemented. To the best of our knowledge, this double combination of hybrid techniques based on RES to provide electricity and heat and desalination to supply fresh water by consuming power or heat has not been tested in depth yet. Therefore, the aim of this paper is to present a selection of the most interesting results coming from the experimental period of a hybrid-sized trigeneration pilot plant which allows providing power, FW and sanitary hot water (SHW) at a much reduced demand scale. As the three demands can be supplied by two complementary techniques, robustness and flexibility makes that plant an interesting solution in isolated areas. Test results show that this scheme is a technically feasible solution (see table 3 and the averaged coverage rate of the three demands in 64 tests). Nevertheless, its profitability and further spreading will depend on realistic economic (that is, without subsidies) and environmental costs of the alternative ways (networks or local transport) to provide the same amounts of energy and water to the study area.

2. Materials and methods

The plant layout of the pilot unit, as well as the final design and predicted productions of power, desalted water by the MD and RO units and SHW was presented in a previous paper (Acevedo et al., 2016). That plant was simulated by TRNSYS® software with weather data from Zaragoza city, located in the northeast of Spain. It was designed to cover the typical electricity and water demands of a four-member Spanish single family home isolated from the grid. Simulations were carried out for a complete year having a time step of 12 min (43.800 iterations). A sensitivity analysis of some design parameters, such that the evacuated tubes collector (ETC) surface, PVT and ETC tilt, hot water tank (HWT) and batteries capacities, heat delivered to the SHW service and mass flow rates feeding the MD unit was also performed. That paper also presented a cost estimation of the power, FW and SHW produced by this pilot unit according to the investment required and lifetime expected. Design was later extended to study the performance and economic benefit in case of having a similar but on-grid trigeneration plant (Bayod-Rújula et al., 2017). Exergy analysis has also been implemented to identify and then to reduce local irreversibilities in the hybrid pilot unit (Acevedo et al., 2017a, 2017b).

The pilot unit has been installed on the roof and the attic of an industrial unit located in the northern Campus of the University of Zaragoza. At this moment, it is operative and isolated from the grid. There are four main subsystems in the plant, as shown in Figure 1. The solar loop is composed of five solar collectors, a solar pump and the HWT. The power loop consists of the supply of the PVT arrays aided with a micro-wind turbine (WT) and the storage on batteries as well as some other auxiliary electric devices. Solar energy collected in the HWT feeds both the SHW demand and the MD unit (SHW loop). Finally, the fresh water loop includes the MD and the RO units, the seawater tank (SWT), feed seawater pumps and associated pipes. Each loop is next described in separated subsections.

Figure 1. Layout of the hybrid trigeneration pilot unit.

2.1. Solar loop

Solar loop consists of four PVT collectors (240 W, 1.63 m^2 each) and one ETC of 3 m^2. The PVTs are divided in two sets connected in series to the ETC, and each PVT set contains two collectors in parallel (2x2). An important amount of the solar irradiation is also transformed into thermal energy to a water-glycol (60/40%) solution that heats a 325 L storage tank (HWT). Heated solution is driven by a pump working upon a hysteresis control loop: it works if the ETC outlet temperature is in the range 7-2ºC above the mean HWT temperature. To avoid overheating in useless periods, an air-cooled heat exchanger (HX-AC) was installed, and the self-emptying of the HWT was also implemented in the control system.

2.2. Power loop

PVTs and batteries are connected by a maximum power point tracker (MPPT) device. A 400 W micro-WT was also connected in parallel with the two lead acid batteries in series (250 Ah, 12 V). Figure 2 shows a picture with the outside equipment of the pilot unit.

Figure 2. Pilot unit RES: WT, PVTs and ETC.

Most of the power from those batteries is converted into AC by means of a regulator/inverter (1 kW). Three pumps are then supplied: solar pump (P_{SL}, 50 W), seawater pump to MD unit (P_{MD}, 80 W) and hot water pump ($P_{HX\text{-}MD}$, 60 W) that feeds the MD by means of a heat exchanger (HX-MD), as well as the HX-AC fan (30 W). Additionally, in order to simulate a variable domestic internal power demand, an AC potentiometer has been installed in the electric cabinet and connected to an electric resistance (ER) of 1 kW. Alternatively, the RO unit consumes DC power from the batteries, and generates up to 30 L/h with very low specific power consumptions (P_{RO}, 110 W) and acceptable salinities (< 300 ppm of TDS). Figure 3 (left) includes the desalting units as well as the electric resistance; on the right picture the electric cabinet, HWT, expansion vessels and batteries are shown.

Figure 3. Detail of the RO and MD units (left) and electric cabinet, HWT and batteries (right).

2.3. SHW loop

Thermal energy stored in the HWT can activate the MD unit (20 L/h max. with a very pure distillate, < 2 ppm of TDS) by means of the abovementioned HX-MD. Alternatively, it can be consumed to serve the SHW demand. The MD pilot unit is a commercial Permeate Gap type (PG) module and contains a spiral wound desalination membrane with a total exchange area of 10 m^2. The PG-MD acts as a countercurrent heat exchanger since the cold side (condenser channel) recovers some heat amount from the hot side (evaporator channel) in the vapor passage across the MD membrane. More details about the performance of this specific MD arrangement can be found from their suppliers (Winter et al., 2011; 2012). Set-up temperature to feed the MD is usually 70ºC, although lower temperatures could activate the unit with reduced distillate rates. Heat flows delivered to MD (Q_{HX-MD}) or SHW (Q_{SHW}) are controlled by a proportional commanded valve (called V1 in Fig. 1). As any SHW discharge from the HWT is usually above the service temperature (45ºC), its blending with tap water was balanced (V2 in Fig. 1) to know the real amount of SHW served to end consumers. The HWT is filled in with tap water only when some SHW demand is served since the one removed to feed the MD unit returns again to the HWT at about 5-6ºC less after transferring the heat. Pump, valves and piping related to this loop could be identified in Figure 4 (left picture).

2.4. Fresh water loop

In order to reduce the pure seawater laboratory samples, a 450 L seawater tank (SWT) was installed to feed both the RO and MD units (Figure 3, left) but also to collect their brines. In terms of salinity, this is not a major problem since salt balance is maintained. However, as MD is a thermal process, brine returns from the MD at warmer temperatures (around 7ºC). Taking into account the reduced recovery ratio (RR) of the MD (about the 2%, that is, brine discharge from the MD is about the 98% of the seawater feed); a significant overheating was then observed in the SWT within the MD operation. Consequently, the MD unit incorporates as a factory design a cooling circuit (a new water-cooled HX consuming tap water, HX-CW) to avoid experimental overheating in the SWT (Figure 4, left).

Nevertheless, since tap water from Zaragoza network is around 30ºC in summer, this HX-CW was not totally useful in this period. Note that RO has to be stopped above 35ºC to protect the membranes, and moreover, MD production is seriously reduced as the temperature drop between hot and cold MD channels is reduced as well. Consequently, for that summer period, the SWT was then additionally cooled by the gradual immersion of 1 L ice jars. A maximum amount of 40 jars were used to help HX-CW in the cooling task, this amount corresponded to the total coverage of the SWT wet grip.

Key operating parameters affecting the MD production in the pilot unit are seawater and SHW flow rates, and HWT and SWT temperatures (hot and cold sinks), having in mind that the driving force in MD is the temperature drop (ΔT_{MD}) between the hot (“evaporator”) and cold (“condenser”) MD channels. Some amount of distillate is then produced according to the transferred heat. Unfortunately, the work of Raluy et al. (2012) is the only one that showed the experience of solar energy coupled to a PG-MD, however flat plate collectors (FPC) were directly linked to the MD module. As a result, an artificial neural network (ANN) was specifically developed by the authors to predict the PGMD distillate as a function of seawater flow rate and seawater temperatures entering the hot and cold MD channels, that is, independently from the heat source type (Acevedo et al., 2018).

2.5. Control and monitoring system

A rather sophisticated control and monitoring system was gradually implemented according to development of tests. Regarding temperature measurement, fourteen PT-100 sensors were installed: three in the solar loop, two in the SHW tank (to check if stratification exists), five for the MD inlets/outlets, two in the HX-MD inlet and return (to assess MD thermal energy consumption) and finally one to measure SWT and outside temperatures respectively. A pyranometer and an anemometer were also installed to compute solar irradiation and wind speed. Finally, a battery controller was connected to the batteries in order to collect voltage, incoming current, charge/discharge rates and state of charge (SOC, %). All those measurements (see table 1 for details and Figure 1 for their positioning) were recorded by the automata every minute, which is also responsible of controlling valves, pumps and fans according to a safe and flexible plant operation.

Unfortunately, plant operation is not fully automatic. Reduced flow rates of the pilot unit are visually measured by six flow meters (water-glycol solution, seawater feed and distillate in MD, permeate in RO, SHW flow to serve HX-MD and SHW demand). Finally, conductivity inside SWT, RO permeate and MD distillate were measured by different conductivity meters, but only the last one (distillate in MD) is recorded by the automata and then managed by the PC (see Fig. 4, right), due to its unsteady behavior.

Figure 4. Detail of the internal SHW circuits (left) and control system (right).

2.6. Uncertainty analysis

According to the methodology proposed by Coleman and Steel (1999), the uncertainty analysis was first conducted by the estimation of the detailed uncertainty of each measured variable *X*, as the addition of its systematic uncertainty (or bias, *B*, mainly related to the accuracy of the instrument and provided by the manufacturers' specifications, after calibration) and random uncertainty (or precision, *P*, related to the repeatability of the measurements), as it can be seen in equation 1.

$$U_X^2 = B_X^2 + P_X^2 \quad (1)$$

Table 1 list the detailed relative uncertainty U of the measured variables in this plant according to the codes previously depicted in Figure 1.

Measurement	Code	Model	Scale	Unit	Readability	B (%)	P (%)	U (%)
Flow rate	F1	NEW FLOW PS-15A-BSP	1-10	L/min	0,2	2.5	2	3.20
	F2	NEW FLOW PS-15A-BSP	1-10		0,2	2.5	2	3.20
	F3	PROFI MESS CA	60-600	L/h	20	5	3.33	6.01
	F4	H2O BEI 20ºC NR-115803	1-24		1	5	4.17	6.51
	F5	BC 52443 A-7	10-80		5	3	6.25	6.93
	F6	TNCO NOVN	1-6	L/min	0,5	5	8.33	9.72
Conductivity	C1	CRISON MM40+	0-500000	µs/cm	0,1	0.5	0.02	0.50
	C2	PCE PHP1	0-200000		0,1	2	0.05	2.00
	C3	PRONTO EC HANNA	0-20	mS/cm	0,01	2	0.05	2.00
Current	I	VICTRON ENERGY BMV-700	0-500	A	0,01	0.40	0.02	0.40
Voltage	V		6,5-95	V	0,01	0.30	0.01	0.30
Charge	Ah		20-999	A·h	0,01			
Batery level	SOC		0-100	%	0,1			
Temperature	T1	PT100 – Class AA*	-30-300	ºC	0,1	0.21	0.033	0.21
	T2				0,1	0.22	0.033	0.22
	T3				0,1	0.25	0.033	0.25
	T4				0,1	0.29	0.033	0.29
	T5				0,1	0.21	0.033	0.21
	T6				0,1	0.19	0.033	0.19
	T7				0,1	0.25	0.033	0.25
	T8				0,1	0.19	0.033	0.19

	T9				0,1	0.27	0.033	0.27
	T10				0,1	0.25	0.033	0.25
	T11				0,1	0.19	0.033	0.19
	T12				0,1	0.27	0.033	0.27
	T13				0,1	0.27	0.033	0.27
	T14				0,1	0.25	0.033	0.25
	T15				0,1	0.25	0.033	0.25
Irradiation	G	LP PYRA 03	0-2000	W/m²	0,01	2.60	0.005	2.60
Wind speed	V	ANEMO4403 4-20 mA	3-180	km/h	1	2.00	0.556	2.08

(*) According to IEC 60751:2008, tolerance values for AA class are ± 0.1+0.0017*T(ºC)

Table 1. Uncertainty analysis of the pilot plant measurements.

Then, the uncertainty U_r of an experimental result $r=r(X_1,X_2,\ldots,X_J)$ can be calculated as a function of the uncertainty of the measured variables X_1 to X_J included in the equation that defines the variable, assuming that they are totally uncorrelated (equation 2).

$$\frac{U_r^2}{r^2} = \left(\frac{X_1}{r}\frac{\partial r}{\partial X_1}\right)^2 \left(\frac{U_{X_1}}{X_1}\right)^2 + \cdots + \left(\frac{X_J}{r}\frac{\partial r}{\partial X_J}\right)^2 \left(\frac{U_{X_J}}{X_J}\right)^2 \qquad (2)$$

Table 2 shows the uncertainty (in relative terms) of the most important performance parameters in the pilot unit. Highest values were found in global energy efficiency of the pilot plant (η_g, 10.76%), thermal efficiency of the PVTs ($\eta_{PVT,t}$, 10.09%) and ETC ($\eta_{ETC,t}$ 10.13%) and heat delivered to SHW (Q_{SHW}, 9.32%). On the contrary, less than the 5% can be found for some other parameters depending on several measurements such as the specific thermal consumption of the MD (SEC_{MD}, 4.68%). Highest uncertainty source comes from the solar loop flow meter (F6), which is then extended to calculations in this loop, followed by the MD and RO flow meters. Note that this rather low accuracy in flow metering is usual in domestic installations where flow meters are not installed.

Parameter	Symbol	Equation	U_r (%)
Power to battery	W	$W = V \cdot I$	0.50
Heat delivered to SHW	Q_{SHW}	$Q_{SHW} = m_{SHW} \cdot Cp_w \cdot (T_{SHW} - T_{tw})$	9.32
Electrical efficiency (PVT)	η_e	$\eta_e = \frac{W_{PVT}}{A_{PVT} \cdot G_S}$	2.65
Thermal efficiency (PVT)	$\eta_{t,PVT}$	$\eta_{PVT,t} = \frac{m_{sl} \cdot Cp_{sl} \cdot (T_{PVT,o} - T_{PVT,i})}{A_{PVT} \cdot G_S}$	10.09
Thermal efficiency (ETC)	$\eta_{t,ETC}$	$\eta_{ETC,t} = \frac{m_{sl} \cdot Cp_{sl} \cdot (T_{ETC,o} - T_{ETC,i})}{A_{ETC} \cdot G_S}$	10.13
Specific energy consumption (MD)	SEC_{MD}	$SEC_{MD} = \frac{Q_{HX-MD}}{F_d} = \frac{m_{HX-MD} \cdot Cp_w \cdot (T_{HX-MD,i} - T_{HX-MD,o})}{F_d}$	4.68
Specific energy consumption (RO)	SEC_{RO}	$SEC_{RO} = \frac{W_{RO}}{F_p}$	2.65
Global energy efficiency	η_g	$\eta_g = \frac{W_{RE} + Q_{SHW} + Q_{HX-MD}}{(A_{PVT} + A_{ETC}) \cdot G_S}$	10.76

Table 2. Uncertainty analysis of the main plant performance parameters.

3. Results

In the period from November 2016 to May 2017, the experimental validation of the single plant devices was carried out (PVT, WT, lead-acid batteries, RO and MD in this order). Especial emphasis was made on the MD tests (see section 2.4); to do that, some MD tests were also carried out independently from the integrated unit, by using the electric resistance (ER) of the HWT.

In May 2017, complete tests started, including the integrated production of power, desalted FW and SHW according to the available renewable energy. Then, from June 2017 the pilot unit was operated to follow as much as possible the power, FW and SHW demands required for a typical family home (4 people). Although several tests have been developed, only main results from the integrated scheme in that last period are presented, in order to analyze the viability and flexibility of the pilot unit based on hybrid RES and desalination techniques.

3.1 Tests based on the RES availability

A short experimental campaign was first developed in May 2017. Trigeneration plant was firstly managed according to the electrical and thermal energy resources available in the pilot unit, in order to test the plant robustness and quick response to control system. This is mainly controlled by the state of charge of the battery (SOC in Fig. 5) and averaged HWT temperature (T_{HWT} in Fig. 5). Those levels were taken into account in order to switch on/off the plant major consumers (RO, MD, SHW and power demands) being the pumps maintained in operation. This period was characterized by a rather good but very instable irradiation (G, see Fig. 5) and breeze (v) corresponding to a typical spring season in Mediterranean climates. In Figure 5, the evolution of the main plant output parameters in a representative day of that period (10/05/2017) is shown. That daytime started at about 9 a.m. (standard time) with a partially cloudy period, even with a light rain, up to noon. The RO unit was switched on (F_p), and the internal power demand was set up to around 500 W (W_h), thus batteries were decreasing its SOC below the 80%, with a rather constant voltage yet (V). Thus, and considering that sunshine appeared, RO was then stopped but MD was put into operation (F_d), thereby in some way substituting permeate by distillate. Power demand was maintained, since irradiation (G) was high at that moment and SOC level was even sustained (see the net power input from RES to batteries, W_{RE}). Suddenly, a storm sharply decreased irradiation at 15 p.m., and therefore MD was stopped since HWT would be drastically reduced in a few minutes. Thus, and although one hour later the sun was shining again, SHW (F_{SHW}) was alternatively served during almost one hour. This was due to that the averaged HWT temperature (T_{HWT}) was yet above the temperature service for HSW, but not enough to maintain the MD unit. At the end of that test, and besides not being a critical threshold, internal power home demand (W_h) was also switched off during the storm since SOC was reduced to 70%.

Figure 5: Experimental test (10/05/2017) following the RES availability.

3.2 Tests following the internal demands

In previous subsection, the operation was tuned to external conditions. Nevertheless, the plant usefulness will depend on the coverage rate of the consumer profiles of power, FW and SHW. Calculation of the demands was based on the typical consumption patterns of a single family home in Spain. Power demand was estimated in 2422,2 kWh per year (REE, 1998) for this housing type. Fresh water demand was estimated in 106,4 cubic meters per year, from this consumption the SHW portion accounts for 37,2 m^3/y (González et al., 2008). Last report was also used to estimate hourly characterization of water and SHW for the averaged day of each month. Existing Spanish regulation (BOE, 2016) for on-grid domestic installations was used to estimate the hourly electricity demand for every day of the year (see table S2 for the two days analyzed in the paper).

From June 2017 the pilot unit is operating to serve power and water demands without any fault. In case of desalted FW, it is assumed that a 1000 L fresh water tank was previously installed in the single family home, thus the RO+MD operation was oriented to fulfill the daily requirements and accordingly, hourly demand is usually exceeded (by far) in daytime tests. However, and bearing in mind that some room of maneuver is available in the batteries and the HWT, hourly profiles for internal power and/or SHW demands were followed at any daytime test. A representative sunny and gentle wind daytime (08/09/2017) is shown in Figure 6, in which main plant output parameters were plotted again. Very high SOC and HWT levels were maintained at the daytime period of that test even if power and water demands were fully covered. In general, when solar irradiation is above 750 W/m^2, the energy balance is positive, in the sense of the internal demands of power, FW and SHW can be covered, and furthermore, some amount of energy can be stored in batteries or in the HWT to be used at nighttime.

Figure 6. Experimental test (08/09/2017) following the scheduled demands.

In the next figure, evolution of solar loop temperatures, as well as the temperatures leaving and returning from the HX-MD and outside temperature along that test are depicted. It can be seen the perfect harmony of HX-MD temperatures with the MD distillate rate (in Figure 6). Moreover, variability found at the solar loop at the sunrise and sundown is typical because of the hysteresis control loop.

Figure 7. Time evolution of some selected temperatures (outside, solar loop and SHW to HX-MD, 08/09/2017).

It is also very interesting to analyze in depth the temporal evolution of the flow temperatures entering and leaving the MD, in order to support the trend observed in distillate rates (Figure 6). As expected, when temperatures in the hot side of the MD (that is, the condenser outlet $T_{cn,o}$ heated by the HX-MD up to the evaporator inlet, $T_{ev,i}$) are elevated with respect to the cold side (condenser inlet $T_{cn,i}$ coming from the SWT after cooling, and evaporator outlet $T_{ev,o}$ returning to the SWT after the heat exchange in the MD), a higher amount of distillate was produced. Those temperatures can be seen in Figure 8, in which the specific thermal energy consumption (SEC, see table 2) of distillate produced is also depicted. Since the amount of heat delivered is more or less the same independently of the HWT temperature (see Figure 7 and HX-MD i/o temperatures), it is obvious that they should be as high as possible to find higher distillate rates, and then lower SEC values.

Figure 8. Time evolution of the MD i/o temperatures and SEC (08/09/2017).

Unfortunately, the continuous operation of the MD unit was provoking a serious overheating in the SWT (see Figure 11). Anyway, temperature of seawater entering the MD ($T_{cn,i}$ in Fig. 8) was stabilized in about 27ºC with the combination of the HX-CW from the MD start up and seawater immersion of the ice jars from 13 p.m. In this manner, the RO can be maintained with the MD up to the full coverage rate of the FW daily demand along the daytime hours (10) of that test. It is fair to say that at that time, seawater flow rate to MD unit (m_{SW}) was reduced from 350 to 300 L/h, being the SHW flow from the HWT ($m_{HX\text{-}MD}$) a constant value of 300 L/h. This can be detected in the small distillate peak at that point (see Figure 6) and therefore a large peak in the SEC value (Figure 8).

Regarding the plant efficiencies (Figure 9), electric efficiency of the PVTs along the test noted the existence of the ETC. The PVTs were operating at quite high temperatures, so rather low values were found, around the 10-11%. In case of thermal efficiency, sunrise and sundown periods were eliminated to avoid detrimental effect on the hysteresis loop. Thermal efficiency of the PVT improves as the irradiation increases along the daytime, however in case of ETC, major losses were found during the early afternoon besides of having better irradiation. For both solar collectors, highest thermal efficiencies were 27 and 18% respectively. Finally, in Figure 9 the overall energy efficiency of the trigeneration unit by linking power and thermal energy, and considering that wind power was not contributing that day (see table 2 for its definition), was also shown. Better figures were in consonance with thermal efficiency in PVTs, at solar noon overall efficiency was around 29%.

Figure 9. PVTs, ETC and global efficiencies of the trigeneration unit (08/09/2017).

Next table includes the most important results of some selected tests in the period from June 2017 to March 2018: time length, productions, and specific consumptions of desalination technologies. Furthermore, in table 3 the coverage rate (CR) of the three demands is also introduced for the same tests, in order to check the plant liability. Last row contains the averaged values of some of the results along the whole set of performed tests in this period (64) following the power, FW and SHW demand.

Table 2. Accumulated productions of some selected daytime tests, and averaged values of the test campaign (64, from June 2017 to March 2018).

Test day	Length (min)	E_{RE} (Wh)	E_h (Wh)	FW_{RO} (L)	FW_{MD} (L)	FW (L)	SHW (L)
06/06/17	412	2005.7	1696.2	183.20	37.78	220.98	74.64
24/07/17	617	3432.5	2340.2	263.42	32.43	295.84	128.95
27/07/17	649	3572.1	2850.9	278.20	24.39	302.59	374.96
08/09/17	581	3664.9	2521.8	239.58	54.02	293.60	50.13
10/10/17	465	3578.1	1799.3	194.73	48.22	242.95	60.02
10/11/17	379	2194.1	1603.2	148.88	33.06	181.94	24.58
30/01/18	244	1447.7	622.9	84.88	27.53	112.41	21.36
22/02/18	314	3982.2	1716.5	127.40	39.55	166.95	28.02
07/03/18	517	3470.4	2410.3	212.08	50.28	262.36	36.95
28/03/18	605	3474.7	2316.8	251.05	50.77	301.82	52.84
Averaged	356	2123.3	1552.1	138.00	29.55	160.20	68.75

Table 3. Demands coverage rate (%), specific consumption in desalination technologies and energy storage variation of the abovementioned tests.

Test day	CR_E (% test)	CR_{FW} (% day)	CR_{SHW} (% test)	SEC_{RO} (kWh_e/m^3)	SEC_{MD} (kWh_t/m^3)	ΔT_{HWT} (ºC)	ΔSOC (%)
06/06/17	96.16	78.19	228.97	3.501	312.65	-7.60	-6.60
24/07/17	101.57	103.96	267.75	3.538	256.63	-5.40	-13.70
27/07/17	91.36	107.11	682.40	3.538	251.35	14.00	-17.50
08/09/17	100.21	103.17	115.34	3.680	303.73	-13.10	-15.80
10/10/17	98.51	88.06	151.03	3.654	306.22	-9.15	-1.60
10/11/17	100.32	59.53	212.09	3.667	329.72	-16.50	-10.40
30/01/18	62.52	39.79	140.88	3.680	258.50	5.80	0.00
22/02/18	98.56	56.36	100.14	3.689	232.49	-10.20	-1.90
07/03/18	99.32	86.26	94.86	3.680	262.69	-1.15	-15.20
28/03/18	99.23	99.49	144.36	3.680	273.00	2.50	-13.80
Averaged				3.656	293.25		

Power, FW as well as SHW demands were perfectly covered every hour, without any major fail detected in the SOC level or HWT temperatures, at least during the daytime of all the performed tests. In some of them, FW and SHW productions could cover the entire daily demand along the daytime test period. Really, the amount of heat required to cover the SHW with respect to the MD requirements is almost negligible, and in 1-2 minutes this demand can be fully covered every hour (see Figure 6). Moreover, and according to the power demands, the full daily power demand could also be covered by nighttime, taking into account the storage capacity of the batteries and considering a minimum SOC of 40% to maintain the battery lifetime. Note that batteries allowed for a range of 1 day and the industrial unit was unavailable at the nighttime period. But it is also noticeable the reduced time window in which the demands could be covered from November to January, sometimes due to the cloudy periods, other times due to partial shading in the industrial unit. In a nutshell, the hybrid plant behavior is rather similar than a solar thermal or PV system, in which a compromise between coverage rate and investment for energy storage and receiving area is adopted in the plant design.

3.3. Economic and environmental costs

Previous design study (Acevedo et al., 2016) estimated power costs in 0.11 €/kWh, and FW and SHW costs in 3.1 and 3.7 €/m^3 respectively. They correspond to the levelized costs of energy and water by considering the investment costs of this pilot unit for a life time of 20 years. Those costs did not consider any environmental bonus related to the use of local RES. Therefore, they are really competitive in a context of an off-grid domestic scheme to supply power and water. To perform a quick comparative analysis, in Spain electricity price for a domestic consumption in the range of 2500 kWh/y is 0.21 €/kWh, and tap water in Mediterranean cities is around 2 €/m^3.

At this point, a comparative environmental assessment based on a Life Cycle Analysis (LCA) of the electricity, FW and SHW provided by this hybrid trigeneration unit in a life cycle of 20 years; and the alternate provision by conventional sources and standardized processes (tap water from the network, power from the Spanish grid and energy mix, and SHW from a domestic natural gas boiler) has been developed. Note that in Acevedo et al. (2016), FW production was not limited in the hybrid scheme and therefore annual FW demand was covered up to 307%, whereas SHW went to the 100% and power was partly covered up to 70%. Thus, new TRNSYS simulations were performed in which those surplus resources consumed in RO were allocated to raise up to 100% the annual electricity demand.

For the case of the hybrid pilot trigeneration plant, a complete Life Cycle Inventory (LCI) was performed with available data from the installation. Environmental impact was calculated by two impact assessment (LCIA) methods (IPCC GWP 2007 and ReciPe) respectively (Pré, 2018; Goedkoop et al., 2013), being the exergy content to cover the entire demand in a year for the three products the adopted criteria to assess the impact among them in a polygeneration scheme. In the case of the conventional supply, environmental impact was assessed by using Ecoinvent processes data base (Weidema et al., 2013) included in the LCIA software SimaPro (Pré Consultants, 2018). Detailed additional information regarding the LCIA methods applied and metrics taken for the conventional supply is included in Suplementary Information file. Comparative values, expressed in kg of equivalent CO_2 per kWh of electricity, or m^3 of FW/SHW (IPCC GWP 2007 method) are in favor of the hybrid RES solution with respect to conventional supply (see Table 4). This reinforces the fact that the hybrid scheme is a sustainable solution, in the sense of 3 times lower specific impacts were found for electricity, and more than 100 times for FW and SHW. Moreover, a presumably conservative option was taken to conventional supply since it was considered that power and water grids could be freely connected to serve the demands; thus environmental transport burdens were not taken into account in the LCIA.

Figure 10 includes the system limits and level of detail of the LCI in the LCA comparison between the renewable and conventional supply. Table 4 introduces as well the weight of the LCIA results between the pilot plant subsystems due to the assembly phase. By LCIA phases, construction (or assembly) LCIA phase accounts for the 7.5% of the total environmental impact of materials and works, being operating phase negligible and dismantle LCIA the remaining 92.5% of the total impact according to the end use of lead acid batteries (Liu et al., 2015). For the conventional supply, as stated in the detailed process analysis (tap water, on-grid power or SHW supply), assembly and operation were representatives, being dismantle phase not considered in the LCA analysis (see supplementary information for more details).

Figure 10. System boundaries and analyzed subsystems of the comparative LCA applied: hybrid-based RES vs conventional supply.

Table 4. Main results of the LCIA comparing the hybrid pilot unit and the conventional supply.

	Product / LCA subsystem	Hybrid RES plant	Conventional
Exergy content to demand (kWh/y):	E_h	2711	
	FW	76.86	
	SHW	139.26	
kg CO_2 equivalent to (20 years):	E_h	13663.4	36332.4
	FW	357.6	663
	SHW	701.9	7337.2
Specific emission (kg $CO_{2,equiv}$/-) per:	E_h (-/kWh_h)	0.002	0.311
	FW (-/m^3_{FW})	0.234	0.670
	SHW (-/m^3_{SHW})	0.003	9.849
Environm. impact (%) due to block:	Solar loop	48.90	
(see Fig. 10)	Wind system	0.67	
	Power storage	28.80	
	Piping & wires	8.22	
	HWT	6.39	
	RO	1.50	
	MD	5.45	

4. Discussion

Tests performed during the autumn and winter season were especially interesting to check if PVTs and WT can maintain safe SOC levels, as well as if MD can be activated or not. Gathered data indicate that both could be maintained but they should be reduced as the daytime period is. The most unexpected result found in lab tests was the scarce power supply from the WT unit with respect to PVT panels, being only representative at nighttime and low SOC levels on the batteries, this was mainly due to the non-manipulable charge controller and difficult positioning of this domestic WT (see figures S1 and S2 in supplementary information). Moreover, the potentiometer had a low efficiency, being the mean difference between the displayed power value served and the one provided from the battery of about 15%.

Additional contingency was the supplementary ice cooling system required in summer to avoid SWT overheating, since it provoked a more complicated development of the tests. Anyway, it should be noted that the abovementioned circumstances are only found in a pilot unit with a single SWT to both feed seawater and collect the brines from desalting units, but this will not occur in the case of a pre-commercial unit directly connected to open seawater for the intake and outfall. On the other hand, the typical HWT set point (70ºC) to activate the MD unit can be reduced in winter season because of the low SWT temperature (about 15ºC). As the driving force to produce distillate (ΔT_{MD}) is almost the same that in summer even when the HWT temperature is below 60ºC, similar distillate rates in both periods can be found.

Regarding the comparison between the two desalting units, it is important to remark that the rate of distillate produced in the MD (F_d) with respect to RO permeate (F_p) is around 1:5 in all tests that MD could be activated. Furthermore, the MD unit takes about 20 minutes to produce some amount of distillate, being RO permeate produced in only a few seconds. Moreover, conductivity of the MD distillate is off-spec (that is, with a higher conductivity than water drinking standards of 1000 mg/L of TDS recommended by the WHO, 2017) in a period of about 30 minutes, having the RO permeate a constant and drinkable value almost from the beginning (see Figure 11 for a comparative qualitative analysis of both products). What is more, higher investment cost of MD with regard to the alternative solution (FW costs should be reduced up to 1.1 €/m^3 by only using the RO), and specific energy consumption found in the tests (250 kWh$_t$/m^3 versus 4 kWh$_e$/m^3) are not in favor of MD. Consequently, and in order to simplify the trigeneration scheme in the hybrid desalting option, even at the expense of a lower water security, the MD (and the ETC) could be dismantled. Nevertheless, that heat surplus not dedicated to MD should be consumed in any other internal purposes like space heating and cooling (by absorption/adsorption chillers and/or heat pumps), thus having a complete off-grid RES-based polygeneration system.

Figure 11. Comparative conductivity analysis of MD and RO (08/09/2017) and SWT temperature.

Scientific literature already mentioned could not be technically compared with the present hybrid plant in terms of performances and efficiencies, since different arrangements and sizes were presented. Something similar occurs with a comparative cost analysis but some reference values are included, despite the fact that most of the works include the economic analysis in terms of the benefits from external prices (Rubio et al., 2011), payback period (Calise et al., 2014; Mohan et al., 2016b) or cost rates ($/h) (Rashidi and Khorshidi, 2018). Specific costs for similar polygeneration schemes based on RES are also very scarce. Two works could only be cited, but both included cooling and are referred to huge-sized configurations. Thus, Leiva et al. (2017) gave cost of 0.1058 USD/kWh for electricity, 2.746 USD/m^3 for water, 0.036 USD/kWh for cooling and 0.024 USD/kWh for heating in a scheme based on CSP (55 MW$_e$) for power and heat, and MED (37,000 m^3/day) for desalination; and Calise et al. (2016) obtained in the optimization of a scheme based on PTC+ORC (1.2 MW$_e$) and MED, some averaged costs along the year of 0.16 €/kWh for electricity, 0.45 €/m^3 for water, 0.187 €/kWh for cooling and 0.017 €/kWh for heating. Exergoeconomic analysis was used in both cases to assess the multiproduct scheme based on solar energy.

Finally, and in order to optimize the cost operation, a procedure has been implemented in the control system to prioritize the service of power, FW or SHW according to the economic benefit obtained from the production of each demand with respect to the supply cost. In this sense, the previous study that estimated the power, FW and SHW costs was used to calculate the benefit of the three products. This means that in case of reaching to unsafe SOC and HWT temperature levels, the plant management will first choose the most profitable production (in €/h) of power, water (by consuming heat or power) or SHW.

5. Conclusions

The hybrid pilot plant based on RES tested at Zaragoza (Spain) allows to completely cover the typical demands of power, FW and SHW of a single family home in summer daytime periods. Total coverage in colder periods is not totally guaranteed. Anyway, total daily demands could be covered by increasing the solar field (PVT panels) and energy storage capacity in batteries and HWT, thereby also increasing the number of episodes in which heat excess has to be evacuated.

Furthermore, the hybrid combination of the MD and RO provides a better management of the available heat and power coming from the PVTs. Complementary fresh water provision is also obtained. Moreover, installed control permits a flexible and safe management of the plant according to diverse objectives, including the economic profitability of its operation depending on external power, fuel and water prices. Tests performed also demonstrated a safe and reliable system for 64 days through the 12 months of one year. Thus, it should be considered as a sustainable solution for the domestic sector in off-grid areas, bearing in mind the reduced environmental impact of this alternative with respect to conventional supply. On the other hand, heat delivered to the MD unit could also be alternatively consumed in HVAC domestic systems, giving the chance to complement the cooling and heating option for this isolated house.

A detailed validation of the TRNSYS simulations with single daily tests is being carried out, in the sense of adapting simulation to real test constraints. One example can be the HWT temperature that activates the MD unit. This fine tuning between the experimental and predicted results will help to find out a validated simulation tool. Thus, the scale-up of this hybrid trigeneration scheme to any other demand profiles, taking into account the plant modularity, could be carried out in the design phase before its implementation. It is noteworthy to remark that the main unit producing blocks (number of PVT, ETC, WT, RO) are modular and the capacities of the batteries and HWT can be easily adopted to some required higher demands, with expect reduced production costs due to economies of scale.

Acknowledgements

The authors wish to thank the financial support given by the Spanish Ministry of Economics and Competiveness in the framework of the “Retos de la Sociedad” R+D Program, under the TRHIBERDE R+D project (ENE2014-59947-R).

References

Acevedo, L., Uche, J., Del Almo, A., Círez, F., Usón, S., Martínez, A., Guedea, I., 2016. Dynamic simulation of a trigeneration scheme for domestic purposes based on hybrid techniques. Energies 9, 1013.

Acevedo, L., Uche, J., Del Almo, A., 2018. Improving the distillate prediction of a membrane distillation unit in a trigeneration scheme by using Artificial Neural Networks. Water 10, 310.

Acevedo, L., Uche, J., Usón, S., Cirez, F., Martínez, A., Bayod, A., Jiang, G., 2017a. Exergy analysis of the transient simulation of a renewable-based trigeneration scheme for domestic water and energy supply. In 10th BIWAES Biennial International Workshop Advances in Energy Studies, Naples, Italy, 25–28 September 2017, Graz University of Technology, Austria.

Acevedo, L., Uche, J., Usón, S., Jiang, G., Del Amo, A., Martínez, A., Bayod, A., 2017b. Modelling and simulating a trigeneration plant: Coupling exergy analysis and Trnsys simulation by the creation of new types. In Proceedings of the International Conference on Energy, Environment and Economics, 15–17 August 2017, Edinburgh, Scotland.

Ahmadi. P., Dincer, I., Rosen, M. A., 2014. Multi-objective optimization of a novel solar-based multigeneration energy system. Solar Energy 108, 576–591.

Al-Ali, M., Dincer I., 2014. Energetic and exergetic studies of a multigenerational solar–geothermal system. Applied Thermal Engineering 71 (1), 16-23.

Al-Karaghouli, A., Kazmerski, L.L., 2013. Energy consumption and water production cost of conventional and renewable-energy-powered desalination processes. Renewable and Sustainable Energy Reviews 24, 343–356.

Bakic, V., Pezo, M., Stevanovic, Z., Zivkovic, M., Grubor, B., 2012. Dynamical simulation of PV/wind hybrid energy conversion system. Energy 45, 324-328.

Banat, F., Jwaied, N., 2008. Exergy analysis of desalination by solar-powered membrane distillation units. Desalination 230, 27-40.

Bayod-Rújula, A.A., Martínez, A., Acevedo, L., Uche, J., Usón, S., 2017. Improved management of battery and fresh water production in grid connected PVT systems in dwellings. In 10th BIWAES Biennial International Workshop Advances in Energy Studies, Naples, Italy, 25–28 September 2017, Graz University of Technology, Austria.

Boletín Oficial del Estado (BOE-A-2016-12487, in Spanish). Resolución de 28 de diciembre de 2016, de la Dirección General de Política Energética y Minas, por la que se aprueba para el año 2017 el perfil de consumo y el método de cálculo a efectos de liquidación de energía, aplicables para aquellos consumidores tipo 4 y tipo 5 que no dispongan de registro horario de consumo, según el Real Decreto 1110/2007, de 24 de agosto, por el que se aprueba el reglamento unificado de puntos de medida del sistema eléctrico.

Brandoni, C., Bosnjakovic, B., 2017. HOMER analysis of the water and renewable energy nexus for water-stressed urban areas in Sub-Saharan Africa. Journal of Cleaner Production 155, 105-118.

Buonomano, A., Calise F., Vicidomini, M., 2016. Design, simulation and experimental investigation of a solar system based on PV panels and PVT collectors. Energies 9, 497-504.

Caldera, U., Bogdanov, D., Afanasyeva, S., Breyer, C., 2018. Role of seawater desalination in the management of an integrated water and 100% renewable energy based power sector in Saudi Arabia. Water 10, 3.

Calise, F., Dentice d'Accadia, M., Piacentino, A., 2014. A novel solar trigeneration system integrating PVT (photovoltaic/thermal collectors) and SW (seawater) desalination: Dynamic simulation and economic assessment. Energy 67, 129-148.

Calise, F., Dentice d'Accadia, M., Piacentino, A., Vicidomini., M., 2015. Thermoeconomic optimization of a renewable polygeneration system serving a small isolated community. Energies 8, 995-1024.

Calise, F., Dentice d’Accadia, M., Macaluso, A., Piacentino, A., Vanoli, L., 2016. Exergetic and exergoeconomic analysis of a novel hybrid solar–geothermal polygeneration system producing energy and water. Energy Conversion and Management 115, 200–220.

Chafidz, A., Kerme, E.D., Wazeer, I., Khalid Y., Ajbar, A., Al-Zahrani, S.M., 2016. Design and fabrication of a portable and hybrid solar-powered membrane distillation system. Journal of Cleaner Production 133, 631-647.

Chang, H., Lyu, S.G., Tsai, C.M., Chen Y.H., Cheng, T.W., Chou, Y.H, 2012. Experimental and simulation study of a solar thermal driven membrane distillation desalination process. Desalination 286, 400–411.

Chen, Y.H., Li, Y.H., Chang, H., 2012. Optimal design and control of solar driven air gap membrane distillation desalination systems. Applied Energy 100, 193–204.

Cherif, H., Belhadj, J., 2011. Large-scale time evaluation for energy estimation of stand-alone hybrid photovoltaic wind system feeding a reverse osmosis desalination unit. Energy 36 (10), 6058-6067.

Coleman, H.W., Steele, W.G., 1999. Experimentation and uncertainty analysis for engineers, Second Edition. John Wiley & Sons Inc., Canada.

Del Amo, A., Martínez, A., Bayod, A.A., Antoñanza, J., 2017. An innovative urban energy system constituted by a photovoltaic/thermal hybrid solar installation: Design, simulation and monitoring. Applied Energy 186,140-151

Demir M. E., Dincer, I., 2017. Development of an integrated hybrid solar thermal power system with thermoelectric generator for desalination and power production. Desalination 404, 59–71.

Durin, B., Margeta J., 2014. Analysis of the possible use of solar photovoltaic energy in urban water supply systems. Water 6, 1546–1561.

Elzahaby, A.M., Kabeel, A.E., Bassuoni, M.M., Refat, A., Elbar, A., 2016. Direct contact membrane water distillation assisted with solar energy. Energy Conversion and Management 110, 397–406.

Gao P., Zhang, L., Cheng, K., Zhang, H.A., 2007. A new approach to performance analysis of a seawater desalination system by an artificial neural network. Desalination 205, 147-155.

Goedkoop M., Heijungs R., Huijbregts M., De Schriver A., Struijs J., van Zelm R., 2013. ReCiPe 2008. A life cycle impact assessment method which comprises harmonised category indicators at the midpoint and the endpoint level First edition (version 1.08)

González, D., Amigo, J., Suárez, F., 2017. Membrane distillation: Perspectives for sustainable and improved desalination. Renewable and Sustainable Energy Reviews 80, 238–259.

González, F., Rueda, T., Les, S., 2008. Microcomponentes y factores explicativos del consumo doméstico de agua en la Comunidad de Madrid (in Spanish). Cuadernos de I+D+I. Canal de Isabel II. Madrid, Spain.

Gude, V.G., 2015. Energy storage for desalination processes powered by renewable energy and waste heat sources. Applied Energy 137, 877–898.

Huang, Q., Shi, Y., Wang, Y., Lu, L., Cui, Y., 2015. Multi-turbine wind-solar hybrid system. Renewable Energy 76, 401-407.

Iaquaniello, G., Salladini, A., Mari, A., Mabrouk, A., Fath, H., 2014. Concentrating solar power (CSP) system integrated with MED–RO hybrid desalination. Desalination 336, 121–128.

Jana, K., Ray, A., Majoumerd, M.M., Assadi, M., De, S., 2017. Polygeneration as a future sustainable energy solution – A comprehensive review. Applied Energy 202, 88–111.

Kabeel, A.E., Abdelgaied, M., Emad M.S., El-Said, E.M.S., 2017. Study of a solar-driven membrane distillation system: Evaporative cooling effect on performance enhancement, Renewable Energy 106, 192-200.

Kalogirou, S.A., 2005. Seawater desalination using renewable energy sources. Progress in Energy and Combustion Science 31, 242–281.

Kim, Y.D., Thu, K., Ghaffour, N., Ng, C.K., 2013. Performance investigation of a solar-assisted direct contact membrane distillation system. Journal of Membrane Science 427, 345–364.

Koroneos, C., Dompros, A., Roumbas, G., 2007. Renewable energy driven desalination systems modelling. Journal of Cleaner Production 15, 449-464.

Leiva-Illanes, R., Escobar, R, Cardemil, J.M., Alarcón-Padilla, D.C, 2017. Thermoeconomic assessment of a solar polygeneration plant for electricity, water, cooling and heating in high direct normal irradiation conditions. Energy Conversion and Management 151, 538–552.

Liang, R., Zhang, J., Zhou, C., 2015. Dynamic simulation of a novel solar heating system based on hybrid photovoltaic/thermal collectors (PVT). Procedia Engineering 121, 675-683.

Liu W., Sang J., Chen L., Tian J., Zhang H., Olvera-Palma G., 2015. Life cycle assessment of lead-acid batteries used in electric bicycles in China. Journal of Cleaner Production 108, 1149-1156.

Manokar, A.M., Winston, D.P., Kabeel, A.E., Sathyamurthy, R., 2018. Sustainable fresh water and power production by integrating PV panel in inclined solar still. Journal of Cleaner Production 172, 2711-2719.

Maraver, D., Uche, J., Royo, J., 2012. Assessment of high temperature organic Rankine cycle engine for polygeneration with MED desalination: A preliminary approach. Energy Conversion and Management 53 (1), 108-117.

Modi, A., Bühler, F., Andreasen, J.G, Haglind, F., 2017. A review of solar energy based heat and power generation systems. Renewable and Sustainable Energy Reviews 67, 1047–1064.

Mokhtari, H., Sepahv, M., Fasihfar, A., 2016. Thermoeconomic and exergy analysis in using hybrid systems (GT+MED+RO) for desalination of brackish water in Persian Gulf. Desalination 399, 1–15.

Mohan, G., Kumar, U., Pokhrel, M. K., Martin, A., 2016. A novel solar thermal polygeneration system for sustainable production of cooling, clean water and domestic hot water in United Arab Emirates: Dynamic simulation and economic evaluation. Applied Energy 167, 173-188.

Mohan, G., Uday, K., Manoj, K., Martin, A., 2016. Experimental investigation of a novel solar thermal polygeneration plant in United Arab Emirates. Renewable Energy 91, 361-373.

Naseri, A., Bidi, M., Ahmadi, M.H., Saidur, R., 2017. Exergy analysis of a hydrogen and water production process by a solar-driven transcritical CO2 power cycle with Stirling engine. Journal of Cleaner Production 158, 165-181.

Ortega-Delgado, B., García-Rodríguez, L., Alarcón-Padilla, D.C., 2016. Thermoeconomic comparison of integrating seawater desalination processes in a concentrating solar power plant of 5 MWe. Desalination 392, 102–117.

Palenzuela, P., Alarcón-Padilla, D.C, Zaragoza, G., 2015. Large-scale solar desalination by combination with CSP: Techno-economic analysis of different options for the Mediterranean Sea and the Arabian Gulf. Desalination 366, 130–138.

Pré Consultants, 2018. What’s new in SimaPro 8.5. Report version 1.1. Pré Consultants bv, The Netherlands.

Pré, various authors, 2018. SimaPro Database Manual. Methods Library, Report version 4.1. Pré, The Netherlands.

Raluy, R., Schwantes, R., Subiela, V., Peñate, B., Melián, G., Betancort, J., 2012. Operational experience of a solar membrane distillation demonstration plant in Pozo Izquierdo-Gran Canaria Island (Spain). Desalination 290, 1-13.

Rashidi, H., Khorshidi, J., 2018. Exergoeconomic analysis and optimization of a solar based multigeneration system using multiobjective differential evolution algorithm. Journal of Cleaner Production 170, 978-990.

Rensonnet, T., Uche, J., Serra, L., 2007. Simulation and thermoeconomic analysis of different configurations of gas turbine (GT)-based dual-purpose power and desalination plants (DPPDP) and hybrid plants (HP). Energy 32, 1012-1023.

Rubio, C., Uche, J., Martínez, A., Bayod, A.A., 2011. Design optimization of a polygeneration plant fuelled by natural gas and renewable energy sources. Applied Energy 88 (2), 449-457.

Rym, C., Dhaouadi, H., Mhiri, H., Bournot, P.A., 2010. TRNSYS dynamic simulation model for photovoltaic system powering a reverse osmosis desalination unit with solar energy. International Journal of Chemical Reactor Engineering 8, 1-13.

Sahoo, U., Kumar, R., Pant, P.C, Chaudhury, R., 2015. Scope and sustainability of hybrid solar–biomass power plant with cooling, desalination in polygeneration process in India. Renewable and Sustainable Energy Reviews 51, 304-316.

Salcedo, R., Antipova, E., Boer D., Jiménez J., Guillén-Gosálbez, G., 2012. Multi-objective optimization of solar Rankine cycles coupled with reverse osmosis desalination considering economic and life cycle environmental concerns. Desalination 286, 358–371.

Serra, L.M., Lozano, M.A., Ramos, J., Ensinas, A.V., Nebra, S.A., 2009. Polygeneration and efficient use of natural resources. Energy 34 (5), 575–586.

Sharaf, M.A, Nafey, A.S, García-Rodríguez, L., 2011. Exergy and thermo-economic analyses of a combined solar organic cycle with multi effect distillation (MED) desalination process. Desalination 272 (1–3), 135-147.

Sharan, P., Bandyopadhyay, S., 2017. Solar assisted multiple-effect evaporator. Journal of Cleaner Production 142, 2340-2351.

Shim, W.G., He, K., Gray, S., Monn, I.S., 2015. Solar energy assisted direct contact membrane distillation (DCMD) process for seawater desalination. Separation and Purification Technology 143, 94-104.

Srinivas, T., Reddy, B.V., 2014. Hybrid solar–biomass power plant without energy storage. Case Studies in Thermal Engineering 2, 75–81.

Trujillo, A., Domínguez, I., Herrera, T., 2014. Using TRNSYS® simulation to optimize the design of a solar water distillation system. Energy Procedia 57, 2441-2450.

Tummala, A., Velamati, R., 2016. A review on small scale wind turbines. Renewable and Sustainable Energy Reviews 56, 1351-1371.

Red Eléctrica Española, S. A. (REE), 1998. Atlas de la demanda eléctrica. Proyecto INDEL (in Spanish). Madrid.

Weiner, D., Fisher, D., Moses, E., Katz, B., Meron, G., 2011. Operation experience of a solar and wind-powered desalination demonstration plant. Desalination 137, 7-13.

Winter, D., Koschikowsky, J., Wieghaus, M., 2011. Desalination using membrane distillation: Experimental studies on full scale spiral wound modules. Journal of Membrane Science 375, 104–112.

Winter, D., Koschikowsky, J., Ripperger, S., 2012. Desalination using membrane distillation: flux enhancement by feed water deaeration on spiral-wound modules. Journal of Membrane Science 243, 215-224.

Weidema B.P., Bauer C., Hischier R., Mutel C., Nemecek T., Reinhard J., Vadenbo C.O., Wernet G., 2013. Overview and methodology. Data quality guideline for the ecoinvent database version 3. Ecoinvent Report 1(v3). St. Gallen: The ecoinvent Centre.

World Health Organization, 2017. Guidelines for drinking-water quality: fourth edition incorporating the first addendum. Geneva. Licence: CC BY-NC-SA 3.0 IGO.

Zambolin, E., Del Col, D., 2010. Experimental analysis of thermal performance of flat plate and evacuated tube solar collectors in stationary standard and daily conditions. Solar Energy 84, 1382–1396.

Zaragoza, G., Aguirre, A., Burrieza, E., 2014. Efficiency in the use of solar thermal energy of small membrane desalination systems for decentralized water production. Applied Energy 130, 491-499.

ACCEPTED MANUSCRIPT

Zhou, C., Liang, R., Zhang, J., 2017. Optimization design method and experimental validation of a solar PVT cogeneration system based on building energy demand. Energies 10, 1281.

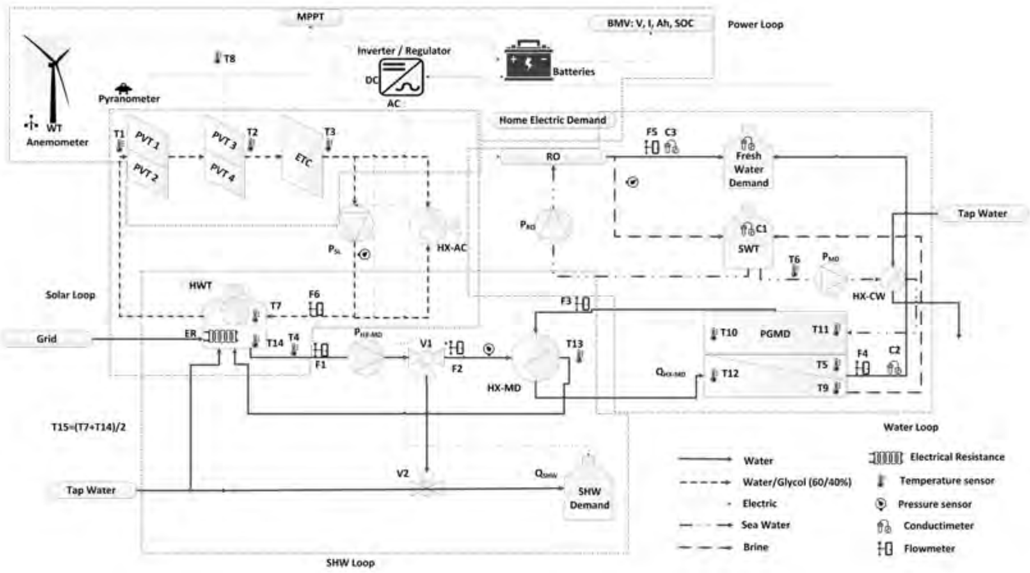
MPPT
BMV: V, I, Ah, SOC
Power Loop
T8
Inverter / Regulator
DC
AC
Batteries
Pyranometer
WT
Anemometer
Home Electric Demand
T1
PVT 1
PVT 2
PVT 3
PVT 4
T2
ETC
T3
RO
F5
C3
Fresh
Water
Demand
Tap Water
PRO
HX-AC
C1
SWT
T6
PMD
HX-CW
Solar Loop
HWT
T7
F6
F3
Grid
ER
T14
T4
F1
PHX-MD
V1
F2
T13
HX-MD
T10
PGMD
T11
F4
C2
QHX-MD
T12
T5
T9
Water Loop
T15=(T7+T14)/2
Tap Water
V2
QSHW
SHW
Demand
SHW Loop
Water
Water/Glycol (60/40%)
Electric
Sea Water
Brine
Electrical Resistance
Temperature sensor
Pressure sensor
Conductimeter
Flowmeter

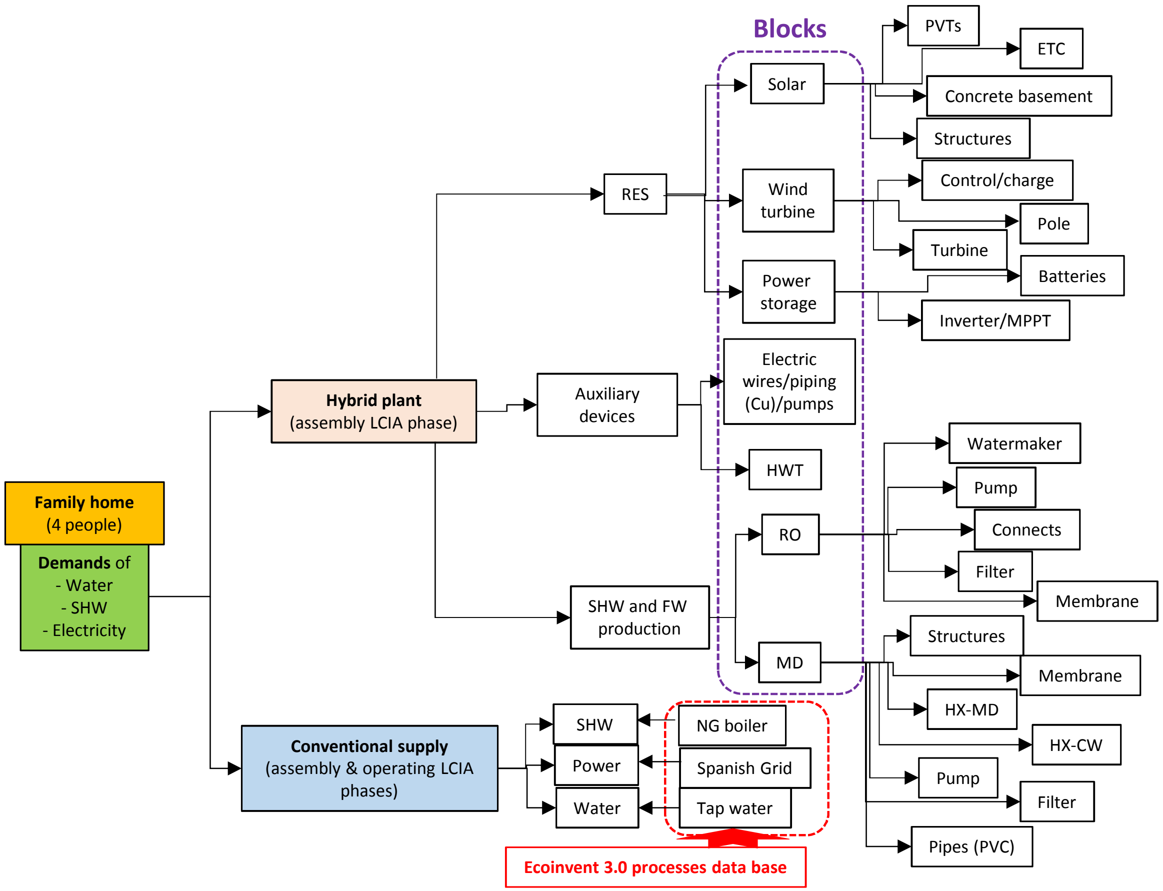
Blocks
PVTs
ETC
Solar
Concrete basement
Structures
Control/charge
RES
Wind turbine
Pole
Turbine
Batteries
Power storage
Inverter/MPPT
Electric wires/piping (Cu)/pumps
Hybrid plant (assembly LCIA phase)
Auxiliary devices
Watermaker
HWT
Pump
Family home (4 people)
RO
Connects
Demands of
- Water
- SHW
- Electricity
Filter
Membrane
SHW and FW production
Structures
MD
Membrane
HX-MD
SHW
NG boiler
HX-CW
Conventional supply (assembly & operating LCIA phases)
Power
Spanish Grid
Pump
Water
Tap water
Filter
Pipes (PVC)
Ecoinvent 3.0 processes data base

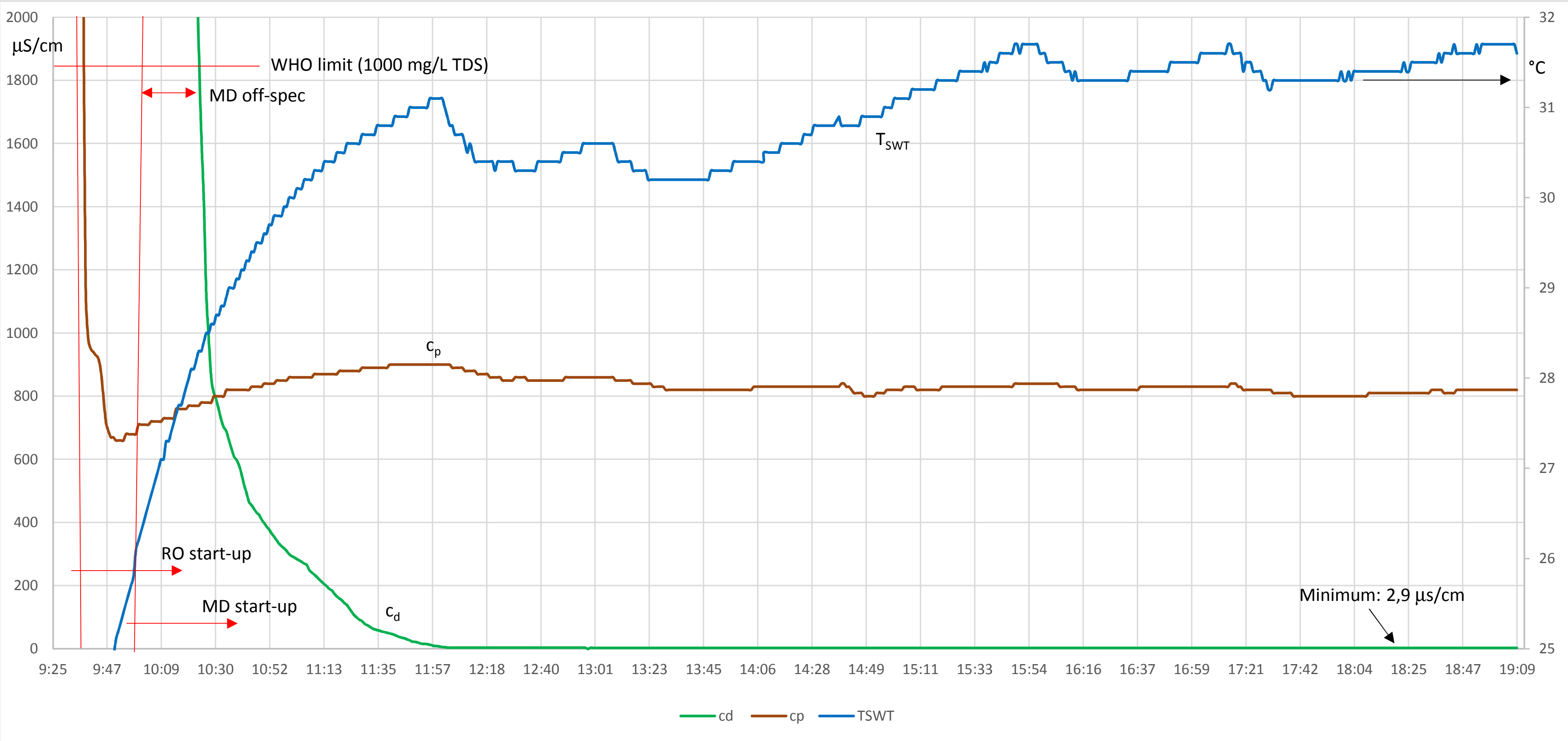

2000
µS/cm
1800
1600
1400
1200
1000
800
600
400
200
0
WHO limit (1000 mg/L TDS)
MD off-spec
RO start-up
MD start-up
c_p
c_d
T_{SWT}
Minimum: 2,9 µs/cm
32
°C
31
30
29
28
27
26
25
9:25
9:47
10:09
10:30
10:52
11:13
11:35
11:57
12:18
12:40
13:01
13:23
13:45
14:06
14:28
14:49
15:11
15:33
15:54
16:16
16:37
16:59
17:21
17:42
18:04
18:25
18:47
19:09
cd
cp
TSWT

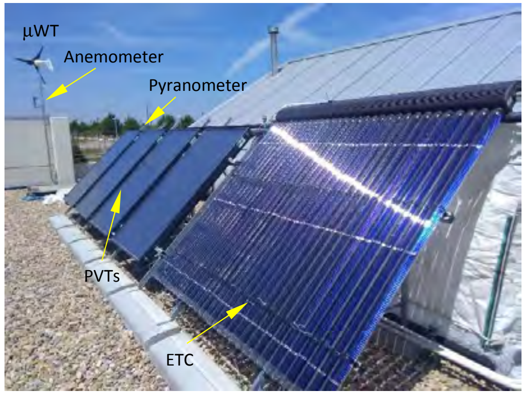
μWT
Anemometer
Pyranometer
PVTs
ETC

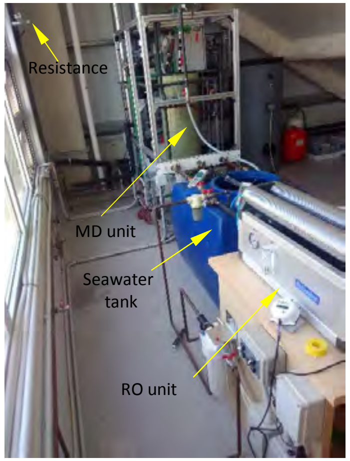
Resistance
MD unit
Seawater
tank
RO unit

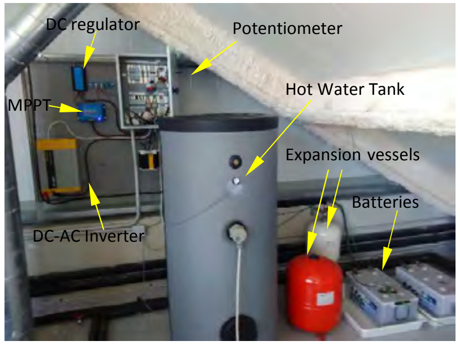
DC regulator
Potentiometer
Hot Water Tank
MPPT
Expansion vessels
Batteries
DC-AC Inverter

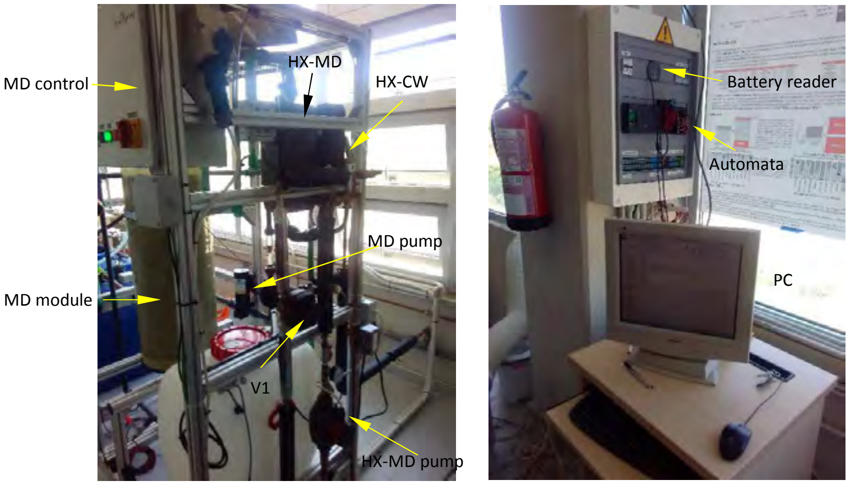
MD control
HX-MD
HX-CW
MD pump
MD module
V1
HX-MD pump
Battery reader
Automata
PC

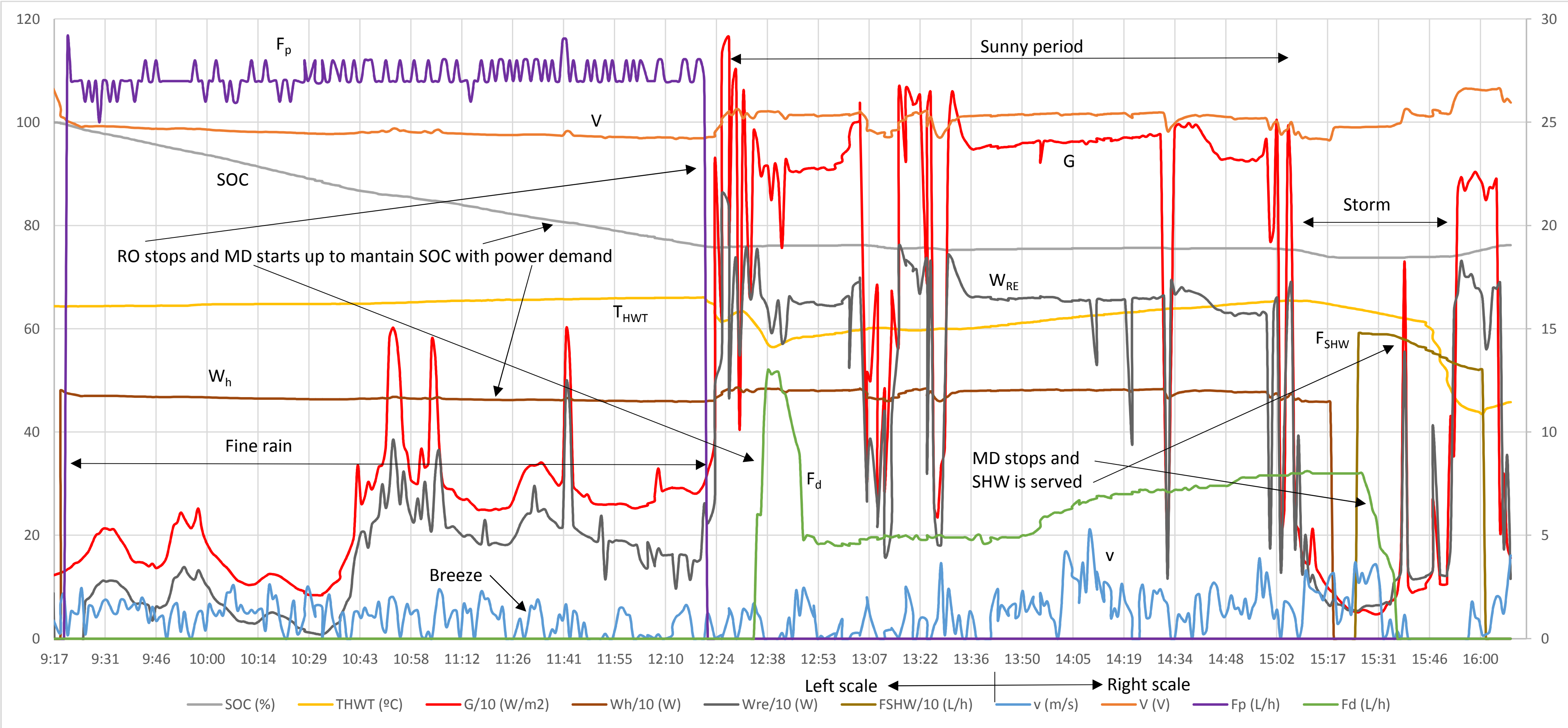

120
100
80
60
40
20
0
30
25
20
15
10
5
0
Fp
Sunny period
V
SOC
G
Storm
RO stops and MD starts up to mantain SOC with power demand
WRE
THWT
FSHW
Wh
Fine rain
MD stops and
SHW is served
Fd
Breeze
v
9:17
9:31
9:46
10:00
10:14
10:29
10:43
10:58
11:12
11:26
11:41
11:55
12:10
12:24
12:38
12:53
13:07
13:22
13:36
13:50
14:05
14:19
14:34
14:48
15:02
15:17
15:31
15:46
16:00
Left scale
Right scale
SOC (%)
THWT (ºC)
G/10 (W/m2)
Wh/10 (W)
Wre/10 (W)
FSHW/10 (L/h)
v (m/s)
V (V)
Fp (L/h)
Fd (L/h)

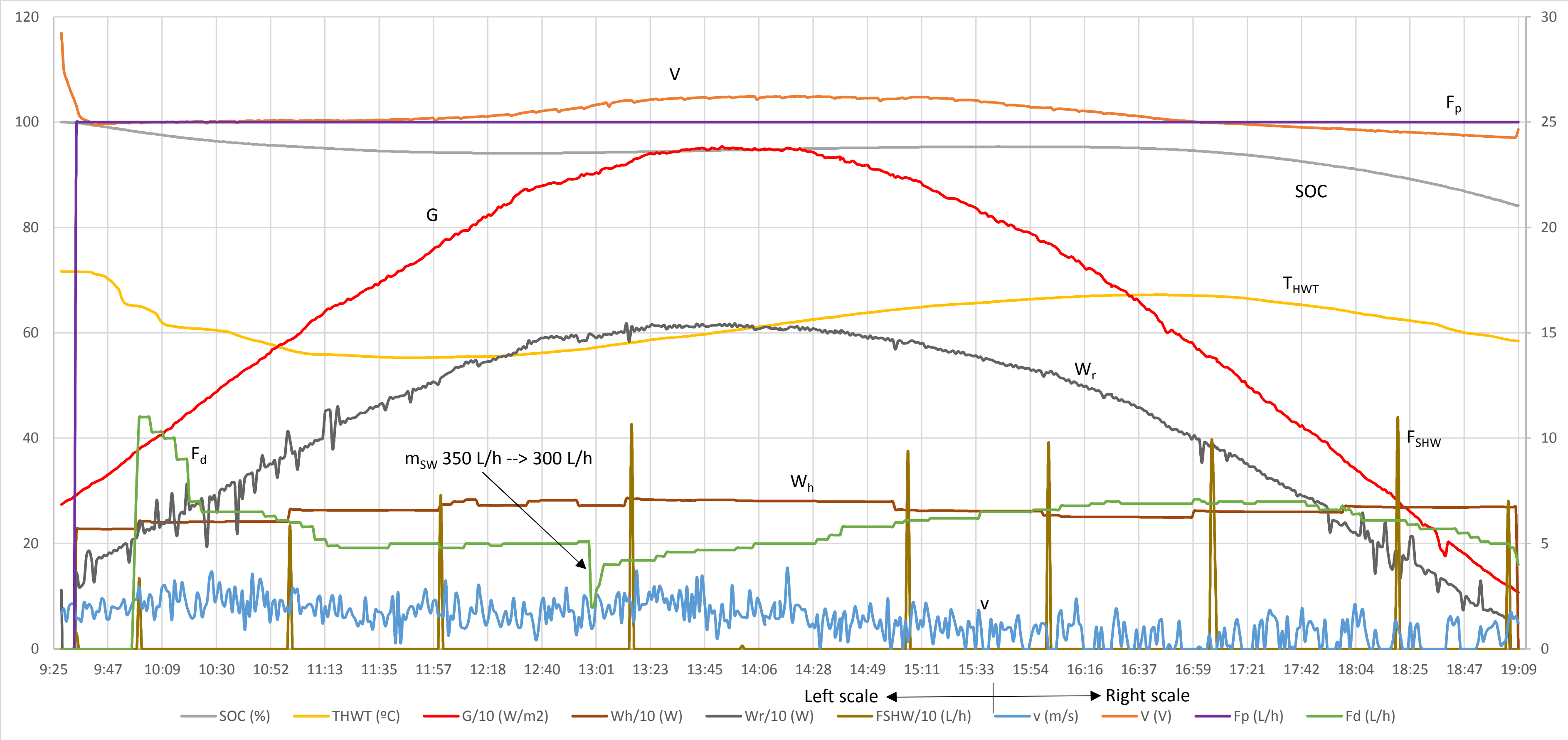

120
100
80
60
40
20
0
30
25
20
15
10
5
0
V
Fp
SOC
G
THWT
Wr
Fd
FSHW
msw 350 L/h --> 300 L/h
Wh
v
9:25
9:47
10:09
10:30
10:52
11:13
11:35
11:57
12:18
12:40
13:01
13:23
13:45
14:06
14:28
14:49
15:11
15:33
15:54
16:16
16:37
16:59
17:21
17:42
18:04
18:25
18:47
19:09
Left scale
Right scale
SOC (%)
THWT (ºC)
G/10 (W/m2)
Wh/10 (W)
Wr/10 (W)
FSHW/10 (L/h)
v (m/s)
V (V)
Fp (L/h)
Fd (L/h)

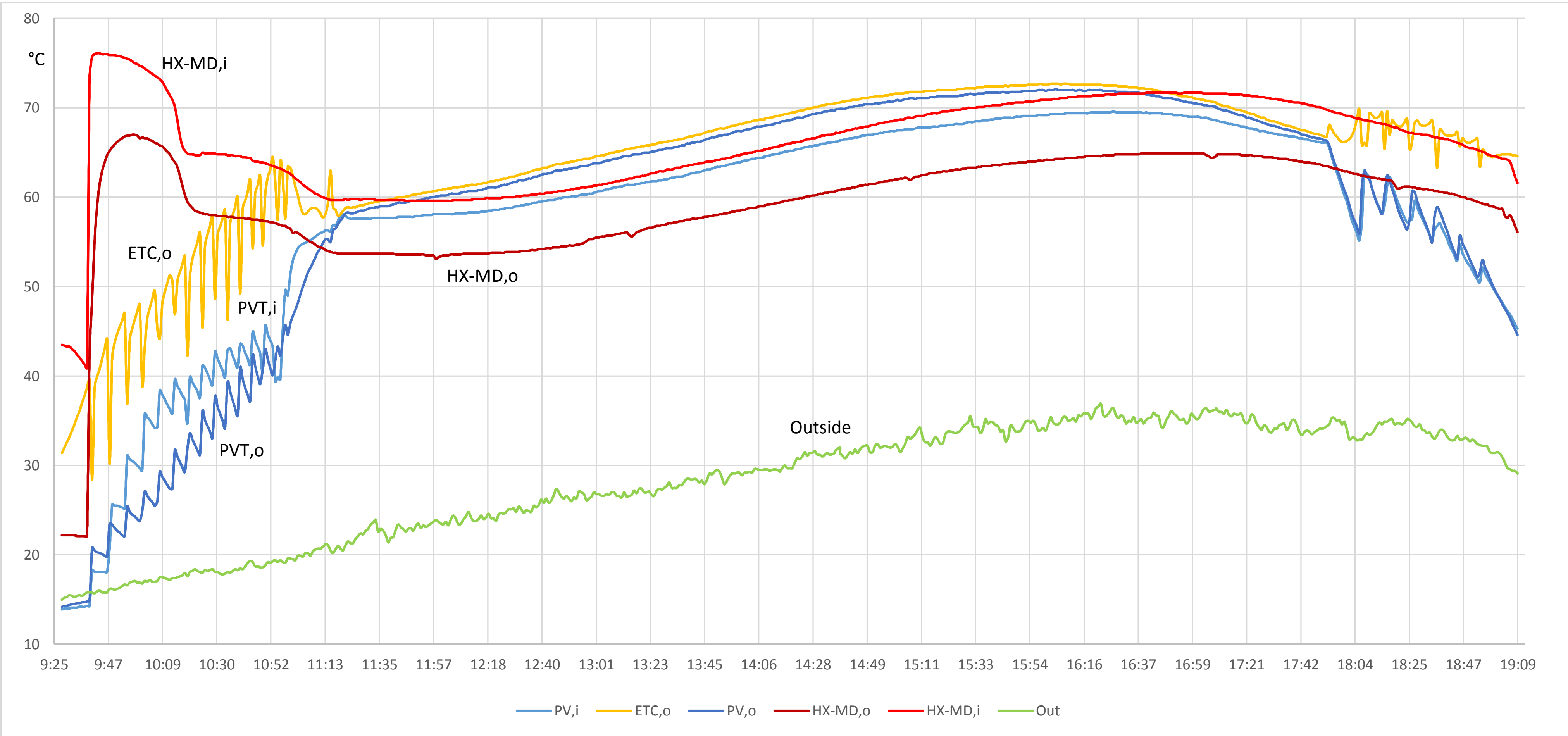
80
°C
70
60
50
40
30
20
10
HX-MD,i
ETC,o
PVT,i
PVT,o
HX-MD,o
Outside
9:25 9:47 10:09 10:30 10:52 11:13 11:35 11:57 12:18 12:40 13:01 13:23 13:45 14:06 14:28 14:49 15:11 15:33 15:54 16:16 16:37 16:59 17:21 17:42 18:04 18:25 18:47 19:09
PV,i ETC,o PV,o HX-MD,o HX-MD,i Out

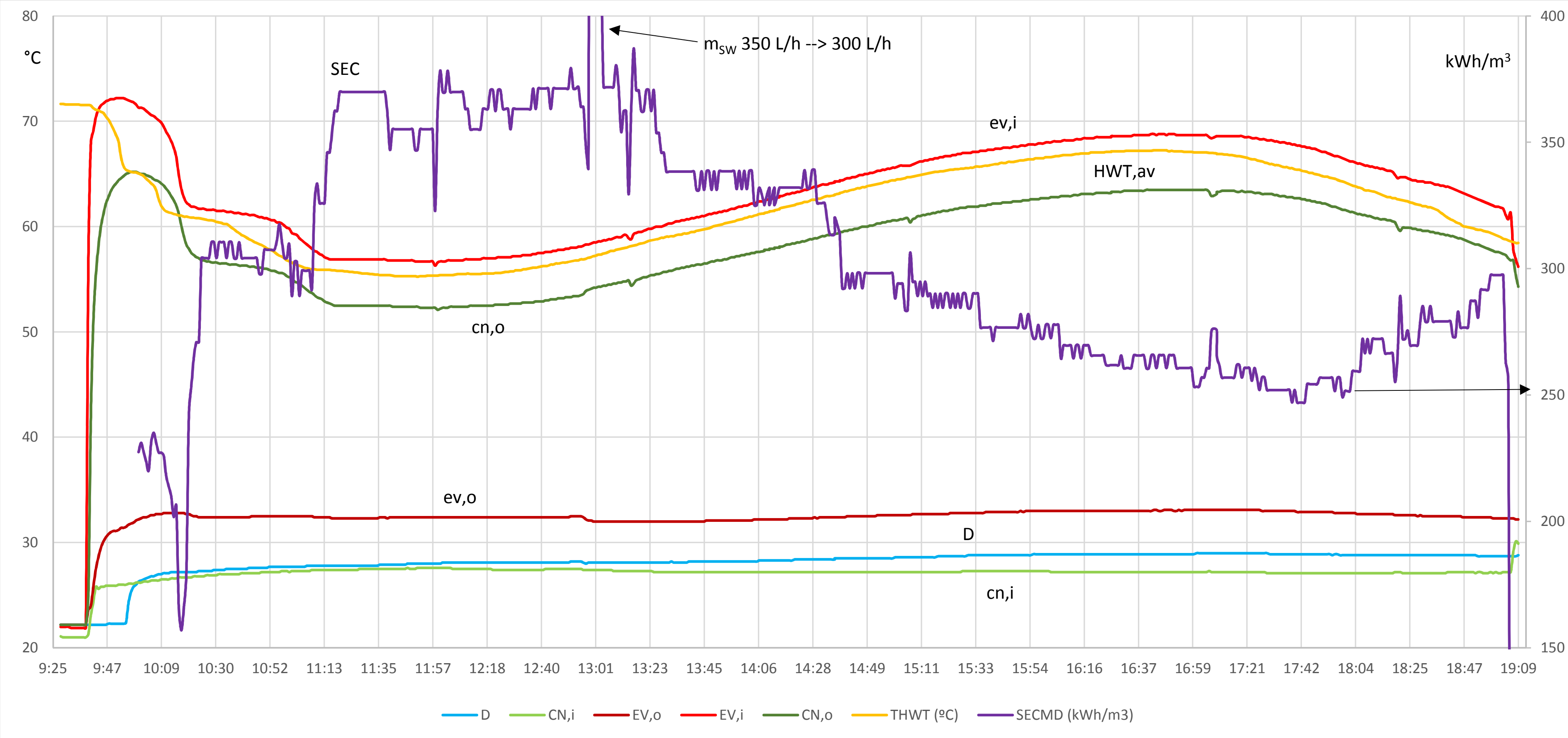

80
70
60
50
40
30
20
°C
400
350
300
250
200
150
kWh/m3
SEC
m_SW 350 L/h --> 300 L/h
ev,i
HWT,av
cn,o
ev,o
D
cn,i
9:25
9:47
10:09
10:30
10:52
11:13
11:35
11:57
12:18
12:40
13:01
13:23
13:45
14:06
14:28
14:49
15:11
15:33
15:54
16:16
16:37
16:59
17:21
17:42
18:04
18:25
18:47
19:09
D
CN,i
EV,o
EV,i
CN,o
THWT (ºC)
SECMD (kWh/m3)

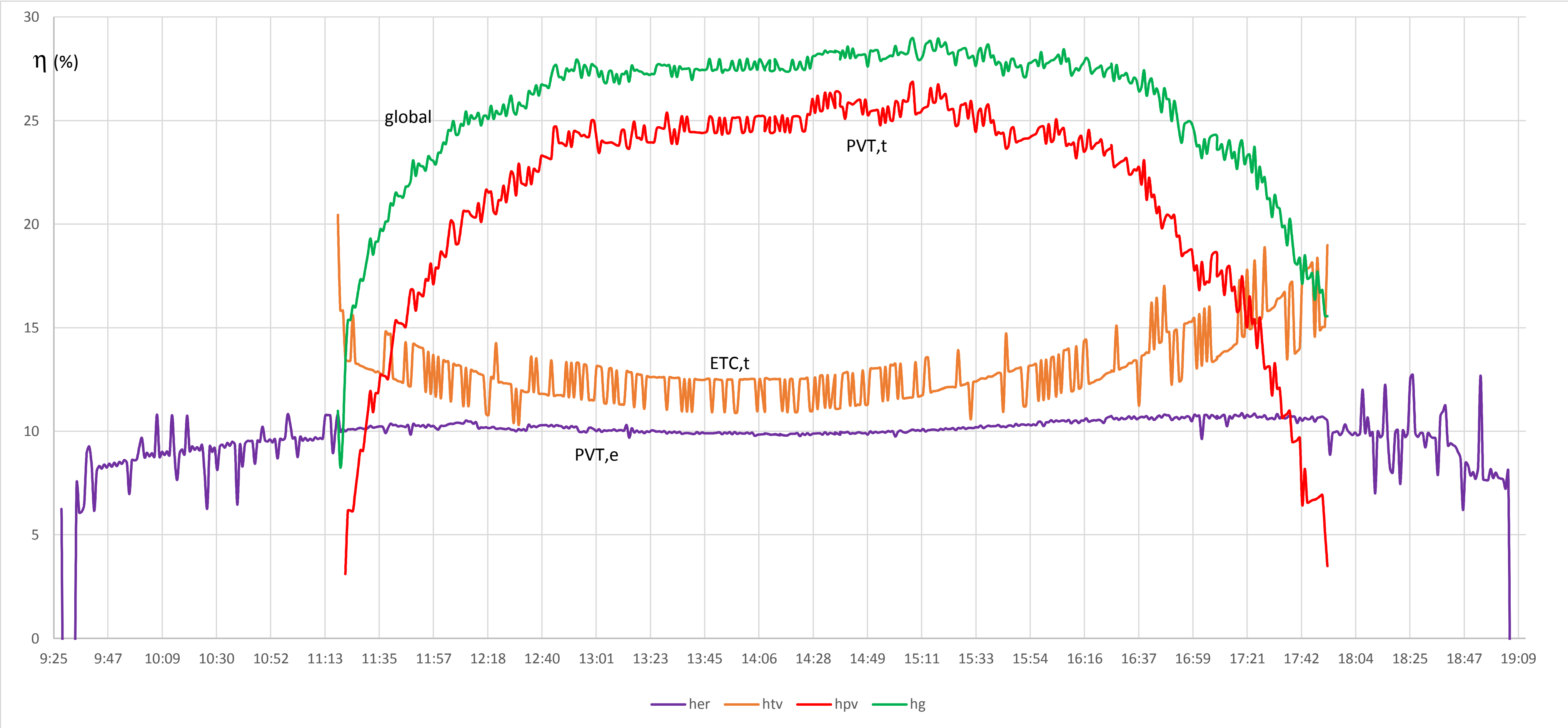

30
25
20
15
10
5
0
η (%)
global
PVT,t
ETC,t
PVT,e
9:25
9:47
10:09
10:30
10:52
11:13
11:35
11:57
12:18
12:40
13:01
13:23
13:45
14:06
14:28
14:49
15:11
15:33
15:54
16:16
16:37
16:59
17:21
17:42
18:04
18:25
18:47
19:09
her
htv
hpv
hg

HIGHLIGHTS:

- Experimental tests of a hybrid trigeneration pilot unit based on RES are presented.
- The test unit provides power, desalted fresh water and SHW for a family of four.
- Average coverage of scheduled demands in daytime tests was found.
- Combined production of power and heat allows a flexible unit.
- Comparative environmental assessment along 20 years life cycle showed low impacts.